

Phase- and angle-sensitive terahertz hot-electron bolometric plasmonic detectors based on FETs with graphene channel and composite h-BN/black-P/h-BN gate layer

V. Ryzhii¹, M. S. Shur², M. Ryzhii³, V. Mitin⁴, C. Tang^{1,5}, and T. Otsuji^{1,1}

¹Research Institute of Electrical Communication, Tohoku University, Sendai 980-8577,

Japan

²Department of Electrical, Computer, and Systems Engineering, Rensselaer Polytechnic Institute, Troy, New York 12180, USA

³Department of Computer Science and Engineering, University of Aizu, Aizu-Wakamatsu 965-8580,

Japan

⁴Department of Electrical Engineering, University at Buffalo, SUNY, Buffalo, New York 14260 USA

⁵Frontier Research Institute for Interdisciplinary Sciences, Tohoku University, Sendai 980-8578,

Japan

We propose and analyze the terahertz (THz) bolometric vector detectors based on the graphene-channel field-effect transistors (GC-FET) with the black-P gate barrier layer or with the composite h-BN/black-P/h-BN gate layer. The phase difference between the signal received by the FET source and drain substantially affects the plasmonic resonances. This results in a resonant variation of the detector response on the incoming THz signal phase shift and the THz radiation angle of incidence.

The specific properties, in particular, the band alignment of graphene and the black-P and black-As (or black-AsP) moderately thick layers¹⁻⁴ enable the operation of different devices using the thermionic electron or hole emission from the graphene channel (GC) via the gate barrier layer (BL). Recently^{5,6}, we predicted that the hot-electron bolometric detectors based on the GC-FETs with the GC and the black-AsP BL can exhibit fairly high characteristics, for example, responsivity. The operation of such detectors is associated with the electron heating by the impinging terahertz (THz) radiation stimulating the thermionic electron emission from the GC via the black-AsP BL into the metal gate (MG). The excitation of the plasmonic oscillations in the gated GC enables the resonant increase in the electron heating reinforcing thermionic emission. Plasmonic resonances can provide elevated detector performance^{5,6}.

The strength of the plasmonic resonances depends on the electron collision frequency ν (determining the plasmonic oscillation damping), i.e., on the electron mobility in the GC. Since the GC contacting the black-AsP exhibits a moderate room temperature mobility (for example,⁷) and not particularly low electron collision frequency, the GC-FETs with the composite h-BN/black-AsP/h-BN gate BLs could be more promising. Indeed, the GC-FETs with the GC main part encapsulated in the h-BN operating at room temperature can provide a fairly pronounced resonant response due to high electron mobility and, therefore, a relatively small ν ^{8,9}. This challenge can be overcome in similar GC-FET bolometric detectors but with the composite incorporating a relatively narrow black-AsP placed between the h-BN side sections. In these detectors, the black-AsP section of the BL serves as the window for the thermionic electron current, while the rest of the h-BN can enable a much weaker electron scattering in the GC. As a result, such GC-FETs can demonstrate a more pronounced resonant response and, hence, elevated responsivity¹⁰.

One of the GC-FET detector's feature is a strong influence

of the signal electric field spatial distribution along the GC on the plasmonic response. This implies that this distribution can be varied by changing the phase difference between the signal voltages created by the antenna system at the GC-FET side contacts (source and drain).

In this paper, we consider the GC-FET bolometric detector structures akin to those proposed and evaluated previously^{5,6,10}, but focusing on their sensitivity to the THz radiation phase and incident angle. Such a property of THz detectors can be useful for different application (see Ref. [11] and the references therein). For the definiteness, we consider the GC-FET bolometric detectors with the GC and the composite h-BN/black-P/h-BN gate BL.

Figure 1(a) shows the GC-FET structures under consideration. The GC-FET comprises the GC sandwiched between the h-BN bottom layer (substrate) and the BL consisting of the lateral h-BN/black-P/h-BN composite. Figure 1(b) shows the GC-FET band diagram at the BL central section (BL window, $|x| \leq L_C$). Here $2L$ is the length of the GC (approximately equal to the MG length), $2L_C$ is the length of the black-AsP section, and the axis x is directed in the GC plane between the side contacts. As an alternative, the WSe₂ side sections of the BL and/or the WSe₂ bottom layer can be used due to the high room temperature mobility¹² (and, hence, a low electron collision frequency) of the GC containing such a BL.

The GC channel is n-doped, so that the electron Fermi energy $\mu \simeq \hbar v_W \sqrt{\pi \Sigma_D} \gg T_0$, where Σ_D is the donor density in the GC or in the neighboring layers, T_0 is the lattice temperature, \hbar is the Planck constant and $v_W \simeq 10^8$ cm/s is the electron velocity in graphene. The material of the MG is chosen to provide the condition $\Delta_M = \Delta_C - \mu_D$, where Δ_C is the difference in the electron affinities of the Al MG and black-P BL and the black-P and the GL. For the black-P BL with the Al MG, $\Delta_M = 85$ meV, $\Delta_C = 225$ meV. The above condition of the proper band alignment is satisfied at $\mu_D = 140$ meV. This corresponds to $\Sigma_D \simeq 1.6 \times 10^{12}$ cm⁻². At elevated bias gate voltages V_G , the electron Fermi energy in the GC μ can

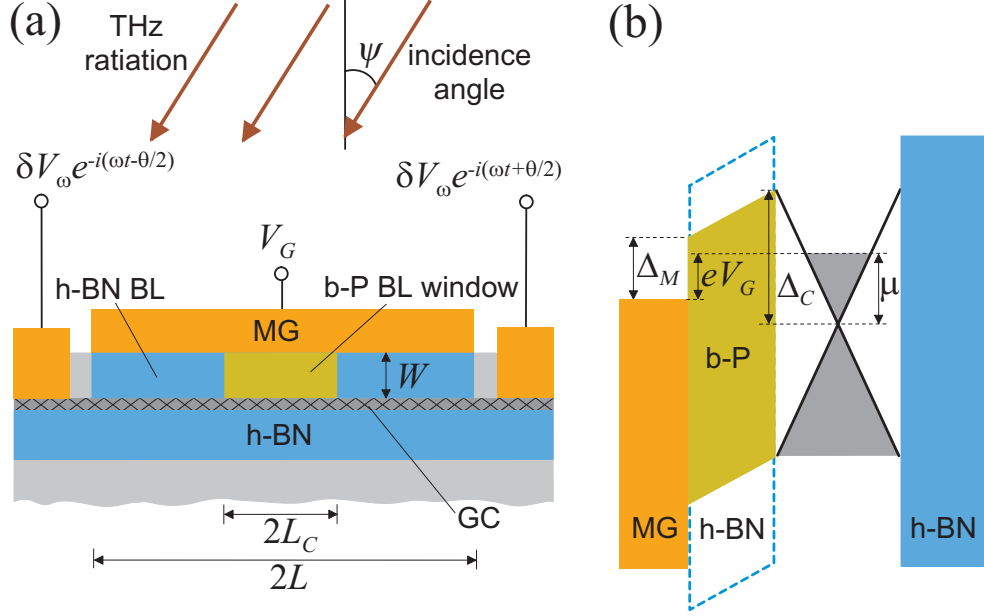


FIG. 1. Schematic view of the structure of (a) GC-FET bolometric detector structure with the composite h-BN/black-P/h-BN BL, (b) band diagram in the central black-P section of the BL (in the BL window; dashed line corresponds to shape of the h-BN BL in the side regions).

somewhat exceed μ_D .

The main distinction of the device under consideration here and that studied previously is the method of the THz radiation input. We assume that the antenna system provides the signal voltages at the source and drain contacts shifted by the phase θ . According to the latter, the signal component GC potential $\delta\phi_\omega$ with respect to the MG potential obeys the following conditions at the edges of the source ($x = -L$) and drain ($x = L$) contacts: $\delta\phi_\omega|_{\pm L} = \delta V_\omega \exp(-i\omega t \pm i\theta/2)$. Here δV_ω and ω are the amplitude and the frequency of the electric signal provided by the antenna system under the effect of the impinging THz radiation, the axis x is directed in the GC plane from the source to the drain, and $2L$ is the spacing between these contacts (approximately equal to the GC length).

The signal voltages at the source and the drain excite the ac electric field δE_ω in the GC causing the absorption of the signal energy by the electrons. The absorbed power per unit of the GC area averaged over the radiation period (the averaging is denoted by the symbol $\langle \dots \rangle$) is equal to the Joule power $Q_\omega = \text{Re} \sigma_\omega \langle \delta E_\omega |^2$, where σ_ω is the GC ac Drude conductivity. The radiation absorption results in the variation, $\langle \delta T_\omega \rangle$, of the effective electron temperature in the GC. The latter leads to the variation of the thermionic currents from the GC via the BL into the MG^{5,6}:

$$\langle \delta J_\omega \rangle^C = H j^{\max} F \int_{-L_C}^{+L_C} dx \frac{\langle \delta T_\omega \rangle}{T_0}. \quad (1)$$

Here $F = (\Delta_M/T_0) \exp(-\Delta_M/T_0)$ is "the thermionic emission factor", $j^{\max} = e\Sigma_D/\tau_\perp$ is the maximal value of the current density from the GC to the MG, τ_\perp is the electron try-to-escape time, and H is the GC width.

In the following, we consider the GC-FETs with $L_C \ll L$. In

these GC-FETs, the plasmonic oscillations resonances in the whole gated GC are primarily attenuated by the electron scattering frequency ν in the GC encapsulated in the h-BN, which can be fairly small^{9,10}, while the effect of a narrow black-AsP window section is weak.

For the axis x spatial distribution of the Joule power associated with the ac electric field produced by the plasmonic oscillations in the gated GC¹³⁻¹⁵, one can obtain

$$\langle Q_\omega \rangle = \frac{\sigma_0}{2} \left(\frac{\delta V_\omega}{L} \right)^2 \left(\frac{\pi \nu}{2\Omega_P} \right)^2 \frac{\omega}{\sqrt{\nu^2 + \omega^2}} \times \left| \left[\frac{\cos(\gamma_\omega x/L) \sin(\theta/2)}{\sin \gamma_\omega} - \frac{\sin(\gamma_\omega x/L) \cos(\theta/2)}{\cos \gamma_\omega} \right] \right|^2. \quad (2)$$

Here $\gamma_\omega = \pi \sqrt{\omega(\omega + i\nu)}/2\Omega_P$ and $\Omega_P = (\pi e/\hbar L) \sqrt{\mu_D W/\kappa}$ is the plasmonic frequency with W and κ being the thickness and dielectric constant of the h-BN/b-P/h-BN BL, respectively. The right-hand side of Eq. (2) describes the resonant overshoots at $\omega \simeq \Omega_P$ and at higher plasmonic resonances.

The spatial distribution of $\langle \delta T_\omega \rangle$ is described by the one-dimensional electron heat transport equation, which for the device structure under consideration is presented in the following form^{5,6}:

$$-h \frac{d^2 \langle \delta T_\omega \rangle}{dx^2} + \frac{\langle \delta T_\omega \rangle}{\tau_\epsilon} = \langle Q_\omega \rangle. \quad (3)$$

Here $h \simeq v_W^2/2\nu$ is the electron thermal conductivity in the GC per electron (this corresponds to the Wiedemann-Franz relation), $v_W \simeq 10^8$ cm/s is the characteristic electron velocity in GCs, τ_ϵ is the electron energy relaxation time in the GC.

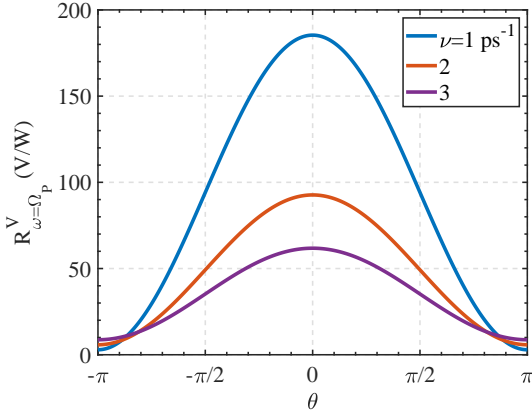


FIG. 2. The GC-FET detector resonant responsivity $R_{\omega=\Omega_p}^V$ as function of phase difference θ at different values of collision frequencies ν .

Equation (3) describes the electron heat propagation along the GC and accounts for the electron heat transfer to the source and drain contacts. The latter can be significant due to high values of the electron heat conductivity^{16,17}. The second term in the left-hand side of Eq. (3) reflects the energy loss by the GC due to its transfer to the lattice^{18–22}. The term describing the electron thermal energy leakage via the BL^{5,6,23} is disregarded because of the small length, $2L_C$, of the window section¹¹. Equation (3) is supplemented by the boundary conditions: $\langle \delta T_\omega \rangle|_{x=\pm L} = 0$.

Since the ac electric field along the GC is not a particularly strongly varying function of the coordinate x , one can replace the right-hand side of Eq. (3) by its spatially averaged value $\langle \overline{Q_\omega} \rangle$ (the Joule power averaged over the GC). Considering the signal frequencies close to the frequency of the fundamental plasmonic resonance and that the quality factor of this resonance $(2\Omega_P/\pi\nu)^2 \gg 1$, we obtain

$$\overline{Q_\omega} \simeq \sigma_0 \left(\frac{\delta V_\omega}{L} \right)^2 \left[\cos^2 \left(\frac{\theta}{2} \right) + \left(\frac{\pi\nu}{4\Omega_P} \right)^2 \sin^2 \left(\frac{\theta}{2} \right) \right] \quad (4)$$

Using Eq. (4), we arrive at the approximate solution of Eq. (3) with the above boundary conditions in the form:

$$\langle \delta T_\omega \rangle \simeq \overline{Q_\omega} \tau_\epsilon \left[1 - \frac{\cosh(x/\mathcal{L})}{\cosh(L/\mathcal{L})} \right], \quad (5)$$

where $\mathcal{L} = \sqrt{\hbar\tau_\epsilon} = v_W \sqrt{\tau_\epsilon/2\nu}$ is the electron cooling length. Equation (5) yields

$$\begin{aligned} \int_{-L_C}^{L_C} dx \langle \delta T_\omega \rangle &\simeq 2\overline{Q_\omega} \tau_\epsilon \left[L_C - \mathcal{L} \frac{\sinh(L_C/\mathcal{L})}{\cosh(L/\mathcal{L})} \right] \\ &\simeq 2L_C \overline{Q_\omega} \tau_\epsilon \left[1 - \frac{1}{\cosh(L/\mathcal{L})} \right]. \end{aligned} \quad (6)$$

The GC-FET bolometric detector voltage responsivity at the fundamental plasmonic resonance is given by $R_{\omega=\Omega_P}^V =$

TABLE I. GC-FET parameters

GC length, $2L$	1.5 μm
Gate layer thickness, W	17.4 nm
Electron Fermi energy, μ	140 meV
Plasmonic frequency, $\Omega_P/2\pi$	1.0 THz
Lattice temperature, T_0	25 meV
Energy relaxation time, τ_ϵ	10 ps
Antenna gain, g	1.64

$(\delta J_{\Omega_P}/S_{\Omega_P})r_L$, where S_{Ω_P} is the power of the normally impinging THz radiation received by the antennas and r_{Load} is the load resistance assumed to be equal to the GC-MG resistance. The quantity $(\delta V_\omega)^2 \propto S_\omega \cos^2 \psi$ (see, for example,²⁴), where ψ is the angle of the radiation incidence. In the case of the normal incidence ($\psi = 0$), using Eqs. (1) and (5) with Eq. (3), we arrive at the following formula:

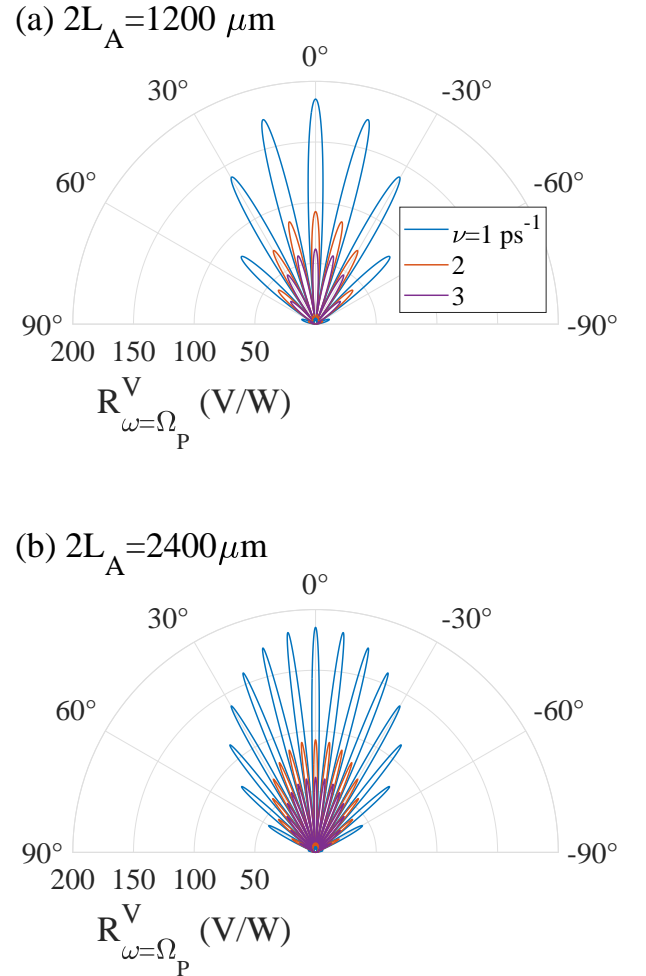


FIG. 3. The GC-FET detector resonant responsivity $R_{\omega=\Omega_P}^V$ as a function of the angle of incidence ψ for different collision frequencies ν for different spacing between the antennas (a) $2L_A = 1200 \mu\text{m}$ and (b) $2L_A = 2400 \mu\text{m}$.

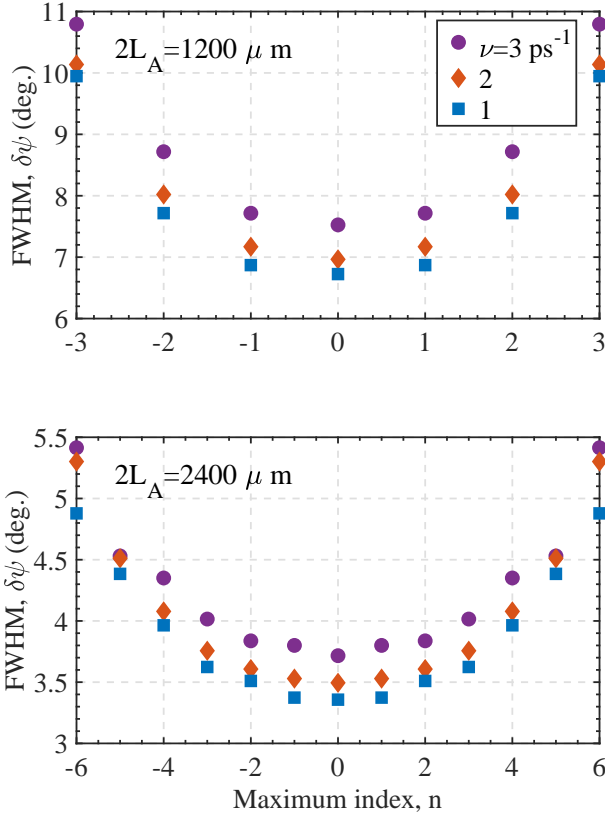


FIG. 4. Angular FWHM of the different peaks of resonant responsivity $R_{\omega=\Omega_p}^V$ corresponding to Fig.3: upper panel - $2L_A = 1200 \mu\text{m}$ and lower panel - $2L_A = 2400 \mu\text{m}$.

$$R_{\omega=\Omega_p}^V \simeq R^V \left[\cos^2\left(\frac{\theta}{2}\right) + \left(\frac{\pi\nu}{4\Omega_p}\right)^2 \sin^2\left(\frac{\theta}{2}\right) \right]. \quad (7)$$

Here

$$R^V = \frac{32}{137g} \left(\frac{\hbar}{eT_0}\right) \left(\frac{\Delta_M}{\mu}\right) \left(\frac{v_W^2 \tau_\epsilon}{L^2 \nu}\right) \left[1 - \frac{1}{\cosh(L/\mathcal{L})}\right]. \quad (8)$$

It is worth noting that R^V is independent of τ_\perp . This is because the GC- to MG THz radiation stimulated current is proportional to τ_\perp^{-1} , while the GC-MG resistance (and, hence, the chosen load resistance) is proportional to τ_\perp .

Figure 2 shows the phase dependence of the resonant voltage responsivity $R_{\omega=\Omega_p}^V$ calculated for the GC-FET bolometric detectors with the band parameters indicated above and characterized by different values of the electron collision frequency ν , i.e., different electron mobilities M . Additional parameters are listed in Table I. One can see that the resonant voltage responsivity can be fairly high at certain values of the phase difference θ , especially in the GC-FETs with relatively small collision frequencies ν (compare, for example, with Refs. [25,26]). The electron mobility in the GC with the values of ν used in Fig. 2 can be estimated as $M \simeq (2.4 - 7.1) \times 10^4 \text{ cm}^2/\text{Vs}$, which is reasonable for GCs encapsulated in n-BN layers.

If the phase shift is associated with the inclined radiation incidence, its value is equal to $\theta = \omega 2L_A \sin \psi / c = 4\pi L_A \sin \psi / \lambda_\omega$, where $2L_A$ is the distance between the antennas producing the voltage signals $\delta V_\omega \exp[-i(\omega t \mp \theta/2)]$ [not shown in Fig. 1(a)] at the source and drain, respectively, c is the speed of light in vacuum, and λ_ω is the THz radiation wavelength. Then we obtain

$$R_{\omega=\Omega_p}^V \simeq R^V \cos^2 \psi \times \left[\cos^2(l_A \sin \psi) + \left(\frac{\pi\nu}{4\Omega_p}\right)^2 \sin^2(l_A \sin \psi) \right], \quad (9)$$

where $l_A = L_A \Omega_p / c$ is proportional to the ratio of the antenna spacing and the impinging THz radiation resonant wavelength and g is the antenna gain. The phase shift can be also associated with the circular polarization of the incident THz radiation²⁷.

Figure 3 demonstrates the angular dependence of the resonant responsivity $R_\omega = \Omega_p^V$ of the detectors with different spacing, L_A , between the antennas calculated for different values of collision frequency ν . As seen in Fig. 3, the angular width of the responsivity peaks is fairly small. This is confirmed by the values of the peaks full width of half maximum (FWHM) shown in Fig.4.

Due to the voltage dependence of the plasmonic frequency Ω_p (associated with the variation of the Fermi energy), the plasmonic resonance can be voltage tuned. This might lead to the controllability of the responsivity phase and incidence angle.

In conclusion, we have proposed the THz GC-FET bolometric detectors with the h-BN/black-P/h-BN BLs and predicted that these detectors can exhibit fairly high room temperature responsivity with a pronounced phase and angular selectivity. Since the detector response strongly depends on the plasmonic resonance (i.e., the ratio ω/Ω_p), the latter is also very sensitive to the impinging radiation frequency.

The work at TU, UoA, and UB was supported by the Japan Society for Promotion of Science (KAKENHI Nos. 21H04546, 20K20349), Japan and the RIEC Nation-Wide Collaborative Research Project No. R04/A10, Japan. The work at RPI was supported by AFOSR (contract number FA9550-19-1-0355).

- ¹Xi Ling, H. Wang, S. Huang, F. Xia, and M. S. Dresselhaus, "The renaissance of black phosphorus," *PNAS* **22**, 4523 (2015).
- ²F. Xia, H. Wang, and Y. Jia, "Rediscovering black phosphorus as an anisotropic layered material for optoelectronics and electronics," *Nat. Commun.* **5**, 4458 (2014).
- ³F. Liu, X. Zhang, P. Gong, T. Wang, K. Yao, S. Zhu, and Y. Lu, "Potential outstanding physical properties of novel black arsenic phosphorus $\text{As}_{0.25}\text{P}_{0.75}/\text{As}_{0.75}\text{P}_{0.25}$ phases: a first-principles investigation," *RSC Adv.* **12**, 3745 (2022).
- ⁴Y. Cai, G. Zhang, and Y.-W. Zhang, "Layer-dependent band alignment and work function of few-layer phosphorene," *Sci. Rep.* **4**, 6677 (2015).
- ⁵V. Ryzhii, C. Tang, T. Otsuji, M. Ryzhii, V. Mitin, and M. S. Shur, "Effect of electron thermal conductivity on resonant plasmonic detection in the metal/black-AsP/graphene FET terahertz hot-electron bolometers," *Phys. Rev. Appl.* **19**, 064033 (2023).
- ⁶V. Ryzhii, C. Tang, T. Otsuji, M. Ryzhii, V. Mitin, and M. S. Shur, "Hot-electron resonant terahertz bolometric detection in the graphene/black-AsP field-effect transistors with a floating gate," *J. Appl. Phys.* **133**, 174501 (2023).

- ⁷Y. Liu, *et al.* “Mediated colossal magnetoresistance in graphene/black phosphorus heterostructures,” *Nano Lett.* **18**, 3377 (2018).
- ⁸A. S. Mayorov, R. V. Gorbachev, S. V. Morozov, L. Britnell, R. Jalil, L. A. Ponomarenko, P. Blake, K. S. Novoselov, K. Watanabe, T. Taniguchi, and A. K. Geim, “Micrometer-scale ballistic transport in encapsulated graphene at room temperature,” *Nano Lett.* **11**, 2396 (2011).
- ⁹M. Yankowitz, *et al.* “Van der Waals heterostructures combining graphene and hexagonal boron nitride,” *Nat. Rev. Phys.* **1**, 112 (2019).
- ¹⁰M. Ryzhii, V. Ryzhii, M. S. Shur, V. Mitin, C. Tang, and T. Otsuji, “Terahertz bolometric detectors based on graphene field-effect transistors with the composite h-BN/black-P/h-BN gate layers using plasmonic resonances,” arXiv:2306.01975v1 (2023).
- ¹¹X. You, Ch. Fumeaux, and W. Withayachumnankul, “Tutorial on broadband transmissive metasurfaces for wavefront and polarization control of terahertz waves,” *J. Appl. Phys.* **131**, 061101 (2022).
- ¹²L. Banszerus, T. Sohler, A. Epping, F. Winkler, F. Libisch, F. Haupt, K. Watanabe, T. Taniguchi, K. Müller-Caspary, N. Marzari, F. Mauri, B. Beschoten, and C. Stampfer, “Extraordinary high room-temperature carrier mobility in graphene-WSe₂ heterostructures,” arXiv:1909.09523v1/.
- ¹³V. Ryzhii, A. Satou, and T. Otsuji, “Plasma waves in two-dimensional electron-hole system in gated graphene heterostructures,” *J. Appl. Phys.* **101**, 024509 (2007).
- ¹⁴V. Ryzhii, T. Otsuji, and M. S. Shur, “Graphene based plasma-wave devices for terahertz applications,” *Appl. Phys. Lett.* **116**, 140501, 2020.
- ¹⁵A. V. Muraviev, S. L. Rumyantsev, G. Liu, A. A. Balandin, W. Knap, and M. S. Shur, “Plasmonic and bolometric terahertz detecti by graphene field-effect transistor,” *Appl. Phys. Lett.* **103**, 181114 (2013).
- ¹⁶T. Y. Kim, C.-H. Park, and N. Marzari, “The electronic thermal conductivity of graphene,” *Nano Lett.* **16**, 2439 (2016).
- ¹⁷Z. Tong, A. Pecchia, C. Yam, T. Dumitrică, and T. Frauenheim “Ultra-high electron thermal conductivity in T-Graphene, Biphenylene, and Net-Graphene,” *Adv. Energy Mater.* **12**, 2200657 (2022)
- ¹⁸J. H Strait, H. Wang, S. Shivaraman, V. Shields, M. Spencer, and F. Rana, “Very slow cooling dynamics of photoexcited carriers in graphene observed by optical-pump terahertz-probe spectroscopy,” *Nano Lett.* **11**, 4902 (2011).
- ¹⁹V. Ryzhii, M. Ryzhii, V. Mitin, A. Satou, and T. Otsuji, “Effect of heating and cooling of photogenerated electron-hole plasma in optically pumped graphene on population inversion,” *Jpn. J. Appl. Phys.* **50**, 094001 (2011).
- ²⁰V. Ryzhii, T. Otsuji, M. Ryzhii, M. Ryzhii, N. Ryabova, S. O. Yurchenko, V. Mitin, and M. S. Shur, “Graphene terahertz uncooled bolometers,” *J. Phys. D: Appl. Phys.* **46**, 065102 (2013).
- ²¹D. Golla, A. Brasington, B. J. LeRoy, and A. Sandhu, “Ultrafast relaxation of hot phonons in graphene-hBN heterostructures,” *APL Mater.* **5**, 056101 (2017).
- ²²K. Tamura, C. Tang, D. Ogiura, K. Suwa, H. Fukidome, Y. Takida, H. Minamide, T. Suemitsu, T. Otsuji, and A. Satou, “Fast and sensitive terahertz detection in a current-driven epitaxial-graphene asymmetric dual-grating-gate FET structure,” *APL Photonics* **7**, 126101 (2022).
- ²³J. F. Rodriguez-Nieva, M. S. Dresselhaus, L. S. Levitov, “Thermionic emission and negative dI/dV in photoactive graphene heterostructures,” *Nano Lett.*, **15** 145 (2015).
- ²⁴R. E. Collin *Antenna and Radiowave Propagation* (New York, McGraw-Hill, 1985).
- ²⁵A. Rogalski, “Semiconductor detectors and focal plane arrays for far-infrared imaging,” *Opto-Electron. Rev.* **21**, 406 (2013).
- ²⁶A. Rogalski, M. Kopytko, and P. Martyniuk, “Two-dimensional infrared and terahertz detectors: Outlook and status,” *Appl. Phys. Rev.* **6**, 021316 (2019).
- ²⁷I. V. Gorbenko, V. Yu. Kacharovskii, and M. S. Shur, “Plasmonic helicity-driven detector of terahertz radiation,” *Phys. Status Solidi RRL*, 1800464 (2018).